SSCL-Preprint-472 Rev. 1

SSCL-Preprint-472 Rev. 1
July 1993
Distribution Category: 414

T. Ogitsu
A. Devred

Influence of Azimuthal Coil Size Variations on Magnetic Field Harmonics of Superconducting Particle Accelerator Magnets

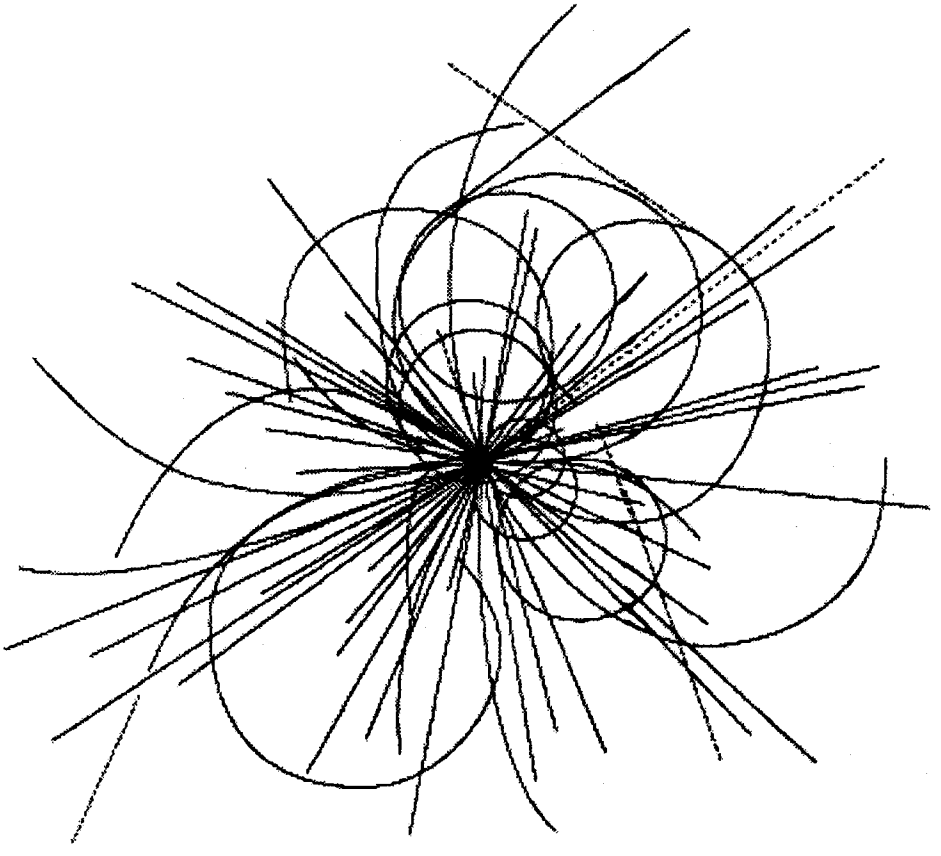

Superconducting Super Collider Laboratory

SSCL-Preprint-472 Rev. 1

Influence of Azimuthal Coil Size Variations on Magnetic Field Harmonics of Superconducting Particle Accelerator Magnets*

T. Ogitsu and A. Devred

Superconducting Super Collider Laboratory†
2550 Beckleymeade Ave.
Dallas, TX 75237

July 1993

*Submitted to the Journal of Applied Physics, July, 1993.

†Operated by the Universities Research Association, Inc., for the U.S. Department of Energy under Contract No. DE–AC35–89ER40486.

Influence of Azimuthal Coil Size Variations on Magnetic Field Harmonics of Superconducting Particle Accelerator Magnets

T. Ogitsu[1,2] and A. Devred[1]

[1]Superconducting Super Collider Laboratory*

2550 Beckleymeade Avenue

Dallas, TX 75237, USA

[2]KEK, National Laboratory for High Energy Physics

1–1 Oho, Tsukuba-shi

Ibaraki-ken, 305, Japan

ABSTRACT

The Superconducting Super Collider (SSC) requires dipole and quadrupole magnets with a very high field quality. The field quality is determined mainly by the dimensions of the magnet coils and their positions with respect to the iron yoke. It is thus very sensitive to manufacturing errors. A model is here developed to estimate the field distortions in a dipole magnet due to azimuthal coil size variations. This model is applied to the data collected during the fabrication and testing of a series of 5 cm aperture, 15 m long SSC dipole magnet prototypes. A clear correlation is observed between the predicted field distortions from the azimuthal coil sizes and the measured skew quadrupole and skew sextupole coefficients.

*Operated by the Universities Research Association, Inc., for the U.S. Department of Energy under Contract No. DE-AC35-89ER40486.

INTRODUCTION

In the long, almost straight, section of a dipole magnet, the field, **B**, can be considered as two-dimensional and is conveniently represented by a multipole expansion

$$\mathbf{B} = B_y + i\,B_x = 10^{-4} B_0 \sum_{n=0}^{\infty} (b_n + i a_n)\left(\frac{x+iy}{r_0}\right)^n, \qquad (1)$$

where B_x and B_y are the x- and y-components of the field, B_0 is the dipole field strength, b_n and a_n are the normal and skew $2(n+1)$-pole coefficients, and r_0 is the reference radius. (For SSC magnets, r_0 = 1 cm.). The rectangular coordinate system (O,x,y,z) is defined so that the z-axis (respectively, the y-axis) is parallel to the beam line (respectively, the normal dipole field), and O is at the beam center (see Figure 1(a)). In Eq. (1), B_0 is in Tesla, and the dimensionless coefficients a_n and b_n are in so-called *units*.

In an ideal dipole magnet, the current distribution is even with respect to the x-axis and odd with respect to the y-axis. These symmetries are such that only even normal multipole coefficients, also called *allowed* multipole coefficients, are expected to be non-zero. In real magnets, however, manufacturing errors result in violations of the dipole symmetries which lead to non-zero *un-allowed* multipole coefficients. For instance, a top/bottom asymmetry in the magnet assembly results in a non-zero a_1 (skew quadrupole coefficient) while a left/right asymmetry results in a non-zero b_1 (normal quadrupole coefficient).[1]

As shown in Figure 1, the SSC dipole magnets use four, saddle-shaped coils which are wound and cured separately and joined during assembly: two *inner* coils (refered to as *upper* and *lower* inner coils) and two *outer* coils (refered to as *upper* and *lower* outer coils). The coil assembly is restrained mechanically by means of laminated, stainless steel *collars*, which are designed to provide a large azimuthal pre-compression as well as to limit the radial deflections caused by the Lorentz force during energization.[2,3] The magnet cold mass is completed by a laminated iron yoke and a stainless steel outer shell. The iron yoke surrounds the collar and

enhances the magnetic field by about 20%. The outer shell is welded around the yoke and delimits the region where the liquid helium circulates.

In this configuration, top/bottom asymmetries can arise from mismatches between the mechanical properties (azimuthal sizes or Young's moduli) of the upper and lower magnet coils. Let us assume that the upper coils are smaller than the lower coils. When mated in the collared-coil assembly, the parting plane, or *midplane*, between the top and bottom coils is shifted upward with respect to the x-axis. This midplane shift results in a current distribution that violates the even symmetry with respect to the x-axis, thus leading to un-allowed multipole coefficients. (Note that there is no practical way to hold the coil parting planes in place, and that midplane shifts can only be avoided by tightly controlling the coil parameters.)

During the fabrication of 5 cm aperture, 15 m long SSC dipole magnet prototypes at Brookhaven National Laboratory (BNL) and Fermi National Accelerator Laboratory (FNAL), systematic azimuthal size measurements were performed along the length and on both sides of the cured coils. These measurements were originally performed to study the mechanics of the collared-coil assembly.[2] After describing how these measurements are taken, we explain how they can be used to estimate the locations of the coil parting planes in the magnet assembly. A model quantifying the influence of coil midplane shifts on magnetic field harmonics is then derived, which we apply to the data collected on the SSC dipole magnet prototypes. Last, we compare the predictions from the model with the results of the magnetic measurements performed on these prototypes. Details on the design, fabrication, and quench performance of the SSC dipole magnet prototypes can be found in references 3 through 7 while reviews of the magnetic measurement data used in this paper are presented in references 8 through 12.

AZIMUTHAL COIL SIZE MEASUREMENTS

Figure 2 shows a picture of the azimuthal coil size measuring device used at BNL. Upon curing completion, the coil is separated from its winding mandrel and is placed on a stable fixture. The fixture incorporates a rail along which the shuttle of Figure 2 is moved manually.

This shuttle carries a concave steel block which supports a short coil length. It also carries three hydraulic cylinders that can azimuthally compress one side of the coil section. At regular intervals, a known pressure is applied to the coil, and the coil azimuthal length is measured. The measurements are first taken along one side of the coil; the shuttle is then flipped; and the measurements are repeated along the other side of the coil. Prior to or after measuring a coil, the device is calibrated using a steel block, called the *master*, which has been accurately machined to the design coil dimensions. All the coil sizes are then referenced to the master. There are, of course, two masters: one used for inner coils and the other for outer coils. At BNL the measurements are taken every 0.75 m under a nominal pressure of 70 MPa for inner coils and 55 MPa for outer coils. At FNAL the coils are measured every 8 cm under a nominal pressure of 84 MPa for both inner and outer coils. The measurement resolution is estimated to be of the order of 10 to 15 μm.

Figures 3(a) through 3(d) present typical examples of azimuthal coil size measurements as a function of axial position for the coils used in SSC/FNAL dipole magnet prototype DCA315. Each trace corresponds to a given side of a given coil. The naming convention is as follows. Coil quadrants are defined by facing the magnet from the *non-lead end*. (The non-lead end is the magnet end opposite to that where the current leads are located.) They are counted counter-clockwise starting from the top-right quadrant (see Figure 1(a)). The sides of the coils are defined by facing the coil from the non-lead end with its curvature down as shown in Figure 1(b). With this orientation, the right-hand side maps into the II/IV quadrants of the final assembly while the left-hand side maps into the I/III quadrants. The axial positions are reckoned from the presumed coil longitudinal center. As can be seen in Figure 3, the peak-to-peak variations in the azimuthal coil sizes are typically of the order of 50 μm.

ESTIMATING COIL MIDPLANE SHIFTS FROM AZIMUTHAL COIL SIZE MEASUREMENTS

Let s_m designate the measured azimuthal size of a given coil under a pressure, σ_m. The spring rate of the coil is known to be a non-linear function of the coil stress.[2] However, for pressures in the 35-80 MPa range, it can be considered as constant. The azimuthal coil size, s, can then be related to the coil stress, σ, and the coil spring rate, k, by

$$\sigma = \sigma_m + k\,(s - s_m). \tag{2}$$

In the collared-coil assembly, the pressure, σ_u, exerted by a given coil of the upper half on the corresponding coil of the lower half, is equal to the pressure, σ_l, exerted by the lower coil on the upper coil. Let s_{um} and s_{lm} designate the measured azimuthal sizes of the upper and lower coils under the pressure σ_m, and let s_u and s_l designate the actual azimuthal coil sizes in the collared-coil assembly. If we neglect frictional effects, σ_u and σ_l can be expressed as a function of s_u and s_l using Eq. (2). From $\sigma_u = \sigma_l$, it can then be shown that

$$(s_u - s_l) = (s_{um} - s_{lm}) - \frac{k_u - k_l}{k_u + k_l}\left[(s_u - s_{um}) + (s_l - s_{lm})\right], \tag{3}$$

where k_u and k_l designate the spring rates of the upper and lower coils, respectively. In practice, the coils are made so that their spring constants are of the same order, *i.e.*, $k_u \approx k_l$. Also, the pressure under which the coil sizes are measured is the target pre-compression for the coil in the collared-coil assembly, *i.e.*, $\sigma_u = \sigma_l \approx \sigma_m$, and thus, $s_u \approx s_{um}$ and $s_l \approx s_{lm}$. It follows that, in first approximation, the second term of the right hand-side of Eq. (3) can be neglected, leading to

$$(s_u - s_l) \approx (s_{um} - s_{lm}). \tag{4}$$

The amplitude of the midplane shift, δ, can thus be estimated to be

$$\delta \approx \frac{s_{um} - s_{lm}}{2}. \tag{5}$$

As an illustration, Figures 3(e) and 3(f) show the amplitude of the midplane shift as a function of z for both sides of the inner layer (solid line) and of the outer layer (dashed line) of SSC/FNAL dipole magnet prototype DCA315.

INFLUENCE OF COIL MIDPLANE SHIFT ON MAGNETIC FIELD HARMONICS

Computing Geometric Field Errors

The transport-current field produced by the coil assembly of a dipole magnet like the one pictured in Figure 1(a) can be calculated by dividing each turn of the coil into elementary current-lines parallel to the z-axis. The field, $\mathbf{B_k}$, generated by such a current line is[1]

$$\mathbf{B_k} = B_{ky} + i\,B_{kx} = -\frac{\mu_0 I_k}{2\pi r_0} \sum_{n=0}^{\infty} \left(\frac{r_0}{\mathbf{z_k}}\right)^{n+1} \left(\frac{x+iy}{r_0}\right)^{n}. \tag{6}$$

Here μ_0 is the magnetic permeability of vacuum, I_k is the current-line intensity, and $\mathbf{z_k} = x_k + iy_k$ is the current-line position in the complex plane. If the current-line is located inside a circular iron yoke of radius, R_y, the contribution of the iron yoke can be shown to be the same as that of a *mirror* current-line of intensity I_k^m and position $\mathbf{z_k^m}$ where[1]

$$I_k^m = \frac{\mu-1}{\mu+1} I_k \tag{7a}$$

and

$$\mathbf{z_k^m} = \frac{R_y^2}{\mathbf{z_k^*}} \quad . \tag{7b}$$

Here μ designates the magnetic permeability of the iron yoke and $\mathbf{z_k^*}$ designates the complex conjugate of $\mathbf{z_k}$. The multipole coefficients of the field produced by the magnet assembly are obtained by summing the contributions of all the elementary current lines. It follows that

$$10^{-4} B_0 (b_n + i a_n) = -\sum_{k=1}^{K} \frac{\mu_0 I_k}{2\pi r_0}\left[\left(\frac{r_0}{\mathbf{z_k}}\right)^{n+1} + \frac{\mu-1}{\mu+1}\left(\frac{r_0\, \mathbf{z_k}^*}{R_y{}^2}\right)^{n+1}\right], \tag{8}$$

where K designates the total number of elementary current-lines. (The conductors used for SSC magnets are Rutherford-type cables made of a few tens of strands, twisted together, and shaped into a flat, slightly keystoned cable.[13] To achieve computational accuracy, the number of current-lines used to represent a given turn of a coil should be of the order of —or larger than— the number of conductor strands.)

In the case of a perfect dipole magnet, the current-line mesh used to compute the field must obey the symmetry rules enunciated in the introduction. Hence, for each current-line (I_k,x_k,y_k) in quadrant I, there should be a current-line $(-I_k,-x_k,y_k)$ in quadrant II, a current-line $(-I_k,-x_k,-y_k)$ in quadrant III, and a current-line $(I_k,x_k,-y_k)$ in quadrant IV. In the following, we shall refer to this mesh as the *perfect-magnet* mesh.

Let us now consider the case where the parting plane between a given side of the upper and lower coils of a given layer is shifted along the y-axis, and let δ designate the amplitude of the shift. The perfect-magnet mesh has to be modified in order to take this shift into account.

Let us first look at a current-line I_k located close to the shifted midplane, and let $\mathbf{z_k} = r_k \exp(i\Theta_k)$ designate the position of I_k in the perfect-magnet mesh. In comparison to the perfect-magnet case, I_k is shifted by δ along the y-axis. Its position, $\mathbf{z_k^s}$, in the shifted mesh can thus be assumed to be

$$\mathbf{z_k^s} \approx \mathbf{z_k} \exp\left(i \arctan \frac{\delta}{r_k}\right), \qquad \Theta_k \approx 0\ . \tag{9}$$

Let us now look at a current-line close to the collar pole face, and let $\Theta_p(r)$ designate the azimuth of the collar pole face at a radius r. (The azimuth varies with the radius because the collar pole face is not radial.) In comparison to the perfect-magnet case, the coil/collar pole face boundary has not moved, and the position of this current-line can be assumed to be the same. Using the same notations as above, we thus have

$$\mathbf{z}_k^s \approx \mathbf{z}_k, \qquad \Theta_k \approx \Theta_p(r_k). \tag{10}$$

Having resolved these two limiting cases, we now have to determine how to modify the positions of the current-lines of azimuth Θ_k, where $0 < \Theta_k < \Theta_p(r_k)$. In the first approximation, the coil can be treated as an homogeneous medium, and the frictional effects can be neglected. Hence, it is reasonable to assume that the midplane shift results in an azimuth change which varies linearly as a function of Θ_k between the two limits given by Eqs. (9) and (10). Using the same notation as above, we thus write

$$\mathbf{z}_k^s \approx \mathbf{z}_k \exp\left[i \frac{\Theta_p(r_k) - \Theta_k}{\Theta_p(r_k)} \arctan \frac{\delta}{r_k} \right], \qquad 0 \le \Theta_k \le \Theta_p(r_k) . \tag{11}$$

Introducing Eq. (11) into Eq. (8) makes it possible to calculate the influence of coil midplane shifts on magnetic field harmonics.

Estimating a_1 and a_2 as a Function of Coil Midplane Shifts

In a dipole magnet, there are four parting planes between upper and lower coils (see Figure 1(a)): 1) between quadrants I and IV of the inner layer, 2) between quadrants I and IV of the outer layer, 3) between quadrants II and III of the inner layer, and 4) between quadrant II and III of the outer layer. Let s_i^{in} through s_{iv}^{in} designate the measured azimuthal sizes of the four inner-coil quadrants, and let s_i^{out} through s_{iv}^{out} designate the measured azimuthal sizes of the four outer-coil quadrants. From Eq. (5) it follows that the amplitudes of the four midplane shifts can be estimated to be $(s_i^{in} - s_{iv}^{in})/2$ and $(s_{ii}^{in} - s_{iii}^{in})/2$ for the inner layer and $(s_i^{out} - s_{iv}^{out})/2$ and $(s_{ii}^{out} - s_{iii}^{out})/2$ for the outer layer. Of course, these midplane shifts are independent, and their combined contributions to a given multipole coefficient is equal to the sum of their individual contributions.

Let the functions $f_{c_n}^{\text{i-iv}}$ and $f_{c_n}^{\text{ii-iii}}$ designate the contributions to a given multipole coefficient, c_n, of the two possible inner-layer midplane shifts, and let the functions $g_{c_n}^{\text{i-iv}}$ and $g_{c_n}^{\text{ii-iii}}$ designate the contributions of the two possible outer-layer midplane shifts. The resulting c_n^s is

$$c_n^s = f_{c_n}^{\text{i-iv}}(s_i^{\text{in}} - s_{iv}^{\text{in}}) + f_{c_n}^{\text{ii-iii}}(s_{ii}^{\text{in}} - s_{iii}^{\text{in}}) + g_{c_n}^{\text{i-iv}}(s_i^{\text{out}} - s_{iv}^{\text{out}}) + g_{c_n}^{\text{ii-iii}}(s_{ii}^{\text{out}} - s_{iii}^{\text{out}}). \quad (12)$$

The functions $f_{c_n}^{\text{i-iv}}$, $f_{c_n}^{\text{ii-iii}}$, $g_{c_n}^{\text{i-iv}}$, and $g_{c_n}^{\text{ii-iii}}$ can be determined numerically using the method described in the previous section. The computation shows that for dipole magnets only the skew quadrupole and skew sextupole coefficients are noticeably affected, and for small midplane shifts, the variations of $f_{c_n}^{\text{i-iv}}$, $f_{c_n}^{\text{ii-iii}}$, $g_{c_n}^{\text{i-iv}}$, and $g_{c_n}^{\text{ii-iii}}$ are quasi-linear. For small midplane shifts, these functions can thus be approximated by their Taylor expansions to the first order, *e.g.*

$$f_{c_n}^{\text{i-iv}}(s_i^{\text{in}} - s_{iv}) \approx f_{c_n}^{\text{i-iv}\,\prime}(0)\,(s_i^{\text{in}} - s_{iv}^{\text{in}}), \quad (13)$$

for small $|s_i^{\text{in}} - s_{iv}^{\text{in}}|$, and the only coefficients to be identified are

$$f_{c_n}^{\text{i-iv}\,\prime}(0), f_{c_n}^{\text{ii-iii}\,\prime}(0), g_{c_n}^{\text{i-iv}\,\prime}(0), \text{ and } g_{c_n}^{\text{ii-iii}\,\prime}(0).$$

The 5 cm aperture SSC dipole magnet prototypes built at BNL and FNAL rely on the same magnetic design.[14] For this magnetic design, the numerical model shows that for midplane shifts less than 100 μm

$$a_1 \approx 8.1\text{x}10^{-3}\,(s_i^{\text{in}} + s_{ii}^{\text{in}} - s_{iii}^{\text{in}} - s_{iv}^{\text{in}}) + 5.5\text{x}10^{-3}\,(s_i^{\text{out}} + s_{ii}^{\text{out}} - s_{iii}^{\text{out}} - s_{iv}^{\text{out}}), \quad (14)$$

and

$$a_2 \approx 1.9\text{x}10^{-3}\,(s_i^{\text{in}} - s_{ii}^{\text{in}} + s_{iii}^{\text{in}} - s_{iv}^{\text{in}}) + 1.3\text{x}10^{-3}\,(s_i^{\text{out}} - s_{ii}^{\text{out}} + s_{iii}^{\text{out}} - s_{iv}^{\text{out}}), \quad (15)$$

where a_1 and a_2 are expressed in units and the coil sizes are expressed in micrometers.

It can be seen in Eq. (14) that the skew quadrupole coefficient is non-zero, if $(s_i + s_{ii})$ is different from $(s_{iii} + s_{iv})$, *e.g.*, if a coil is bigger than the corresponding coil of the other half. For the skew sextupole coefficient, Eq. (15) shows that a non-zero value arises if $(s_i + s_{iii})$ is different

from ($s_{ii} + s_{iv}$), *e.g.*, if one side of the coils is systematically larger than the other side. As an illustration, a top/bottom asymmetry of 100 μm for both sides of the inner coils results in 1.6 units of a_1 while an asymmetry of 100 μm between the II/IV and I/III sides of both upper and lower inner coils results in 0.4 units of a_2. These numbers have to be compared to the design specifications on a_1 and a_2. For particle accelerators, the specifications on multipole coefficients are given in terms of systematic and rms tolerances.[15] The meaning of these specifications is that the average value (respectively, the rms value) over the ensemble of magnets must be less than the systematic tolerance (respectively, the rms tolerance). For the dipole magnets of the SSC main ring, the systematic tolerance on a_1 (respectively, a_2) is 0.04 units (respectively, 0.032 units) while the rms tolerance is 1.25 units (respectively, 0.35 units).[16] The calculated values for deviations of the order of 100 μm thus exceed the rms tolerances, demonstrating the extreme sensitivity of low order un-allowed multipole coefficients on coil size mismatches.

The manufacturing process determining the azimuthal coil sizes is believed to be curing.[2] During curing, the coil and its winding mandrel are laid on a bed of concave, laminated-steel blocks constructed to very accurate dimensions and called *form blocks*. Coil-mandrel assembly and form blocks are covered by steel contact parts, called *top hats*, which are hydraulically pressed. The form blocks are heated until the adhesive of the coil insulation polymerizes, and the top hats are pressed until they come into contact with the form blocks (or with shims of appropriate thicknesses placed on the form blocks). Temperature and pressure are maintained for about 2 hours.

The fact that, as a result of curing, some coils may come out bigger than others is probably unavoidable. However, if the production coils are randomly mixed, there is no reason why the bigger coils would systematically end up in the same halves of the magnet assemblies, *i.e.*, always in the upper half, or always in the lower half. This means that although there may be large magnet-to-magnet variations in both the sign and the amplitude of a_1, nothing in the assembly process is expected to produce a systematic, non-zero value. The situation is different for the skew sextupole coefficient. Let us for instance assume that a curing press is such that the

II/IV side of the coil always comes out bigger than the I/III side. Then when two coils produced on this press are mated, the bigger side of the lower coil is always located in quadrant IV while the bigger side of the upper coil is always located in quadrant II, resulting in midplane shifts, and non-zero a_2, which are always of the same sign. This time, there is a systematic effect which will be reproduced for all the magnets made with coils cured in this press. The way around this problem would be to mix coils cured in different curing presses. The number of curing presses, however, is limited, which limits the possibility of randomizing the process.

COMPARISON BETWEEN MEASUREMENTS AND PREDICTIONS

Measurements of the axial variations of the multipole coefficients (*z-scan*) were performed on all the SSC dipole magnet prototypes that were produced.[8-11] The measurements were taken using the *mole* system developed at BNL.[17] The mole consists of a tangential coil and two dipole bucking windings, which are 0.6 m in length (B2 mole used at FNAL)) or 1.0 m in length (FA series moles used at BNL) and rotate with a 3.2 s period (B2 mole) or a 3.5 s period (FA series moles). The data reported here are from z-scans performed at 4.35 K and 2 kA nominal, after a current standardization cycle to 6.5 kA.[12,18] The current of 2 kA is selected to be in a regime where there is little time decay of the multipole coefficients[18] and where the effects of iron saturation are negligible.[12,19] At each axial position, the multipole coefficients are expressed in a coordinate system where a_0, a_7, and b_7 are forced to be zero. The y-axis of this coordinate system is parallel to the normal dipole field and its origin is believed to be within 50 μm of the magnet mechanical center at the given z position.

The solid line of Figure 4(a) represents a_1 as a function of z as measured on SSC/BNL dipole magnet prototype DCA209, while the solid line of Figure 4(b) represents a_2 as a function of z as measured on SSC/FNAL dipole magnet prototype DCA315. In both figures, the dashed line represents the estimated multipole coefficients from the azimuthal coil sizes. (In comparing the two lines, note that the estimate from the coil sizes corresponds to a local value at a given z, while the mole data corresponds to an average value over the mole length.) For both a_1 and a_2,

the solid and dashed lines appear to follow similar patterns, thus demonstrating the existence of a correlation between coil sizes and low order, un-allowed multipole coefficients.

Figure 5 presents a summary plot of a_2 as a function of z as measured on a series of 5 SSC/FNAL dipole magnet prototypes. It appears that the five traces of Figure 5 follow similar patterns. The axial variations of a_2 are thus somewhat reproducible magnet to magnet. As we elaborated in the previous section, the cause of a_2 is likely to be found in tooling asymmetries which result in left/right asymmetric coils. All the coils assembled in this series of magnets (20 inner and 20 outer) were cured in the same curing press. Figure 6(a) presents a summary plot as a function z of the azimuthal coil size differences between the II/IV side and the I/III side of a representative sample of 5 (upper) inner coils, while Figure 6(b) presents a similar summary plot for a representative sample of 5 (upper) outer coils. As in Figure 5, the five traces of Figures 6(a) and 6(b) appear to follow similar patterns. It also appears that the structure of the inner coil traces of Figure 6(a) is somewhat similar to that of the outer coil traces of Figure 6(b). This suggests that the asymmetry believed to be at the origin of a_2 is in the curing press itself, rather than in the form blocks which contain the coils, and which, of course, are different for inner and outer coils.

Having established that the axial variations of low order, un-allowed multipole coefficients within a magnet could be correlated to the axial variations of the azimuthal coil sizes, we can now take averages over the magnet length and do cross-magnet comparison. Figure 7(a) presents a summary plot of measured a_1 versus estimated a_1 from coil sizes, averaged over the lengths of a series of 5 cm aperture, 15 m long SSC dipole magnet prototypes. (The DCA200 series magnets were produced and cold-tested at BNL while the DCA300 series magnets were produced and cold-tested at FNAL.) Although there is some scatter, a clear correlation can be seen between measured and estimated values. A linear fit, P_1, of the data in Figure 7(a) is

$$a_1^{\mathrm{m}} \approx P_1(a_1^{\mathrm{e}}) = 0.87\, a_1^{\mathrm{e}} + 0.18\,, \tag{16}$$

where a_1^m (respectively, a_1^e) designates the measured (respectively, estimated) a_1 expressed in units. The χ^2 of $(a_1^m - P_1(a_1^e))$ is 0.35. This large χ^2 and the fact that the slope of the linear fit is not equal to 1 indicates that not all of the magnet-to-magnet variations in a_1 can be explained in terms of coil size asymmetries.

Figure 7(b) presents a summary plot of measured a_2 versus estimated a_2 from coil sizes, averaged over the lengths of the same series of magnets. The correlation between measured and estimated values appears to be stronger than for a_1. A linear fit, P_2, of the data in Figure 7(b) is

$$a_2^m \approx P_2(a_2^e) = 0.94\, a_2^e + 0.01, \tag{17}$$

where a_2^m (respectively, a_2^e) designates the measured (respectively, estimated) a_2 expressed in units. The χ^2 of $(a_2^m - P_2(a_2^e))$ is 0.01. This small χ^2 and the fact that the slope of the linear fit is close to 1 indicate that most of the magnet-to-magnet variations in a_2 can indeed be explained in terms of coil size asymmetries.

A remarkable feature of Figures 7(a) and 7(b) is that they mix magnets built at two different factories (BNL and FNAL) and with coils having different conductor insulation. The bulk of these magnets (SSC/BNL magnet DCA207 through DCA211 and SSC/FNAL magnet DCA311 through DCA319) uses a standard Kapton®/epoxy-impregnated fiberglass insulation scheme.[2†] Four of the remaining magnets rely on a so-called *all-Kapton®* insulation scheme with either a polyimide adhesive coating (SSC/BNL magnet DCA212 and DCA213) or a B-stage epoxy coating (SSC/FNAL magnet DCA320 and DCA321).[6] The last two SSC/FNAL magnets (DCA322 and DCA323) also avoid the use of fiberglass, but rely on alternate materials to replace Kapton® and epoxy. In spite of these differences, all the magnets appear to fall along the same lines.

Another remarkable feature of Figure 7(b) can be seen when removing the all-Kapton® and alternate insulation magnets and concentrating on the large sample of standard Kapton®/fiberglass insulation magnets. It appears that although the BNL and FNAL magnets

† Kapton® is a registered trademark of E. I. DuPont de Nemours & Co.

follow the same correlation, the BNL magnets, which all have a positive a_2, are clearly dissociated from the FNAL magnets, which all have a negative a_2. Hence, the averages of the two populations are non-zero and of opposite signs, which leads us to believe that the systematic effects causing the non-zero skew sextupole coefficient are of opposite directions at the two magnet factories. As we described above, a non-zero a_2 is likely to be caused by a left/right asymmetry in the curing press. All the BNL coils, on one hand, and all the FNAL coils, on the other hand, were cured in the same press, but the BNL and FNAL curing presses were different. A plausible explanation for the occurrence of systematic skew sextupole coefficients of opposite signs is thus that the BNL and FNAL presses have left/right asymmetries of opposite directions. (The number of magnets using the other types of insulation is not large enough to draw any significant conclusion.)

CONCLUSION

A model was developed to describe the influence of azimuthal coil size variations on the skew quadrupole and skew sextupole coefficients of superconducting particle accelerator dipole magnets. This model was applied to the data collected during the fabrication and testing of a series of 5 cm aperture, 15 m long SSC dipole magnet prototypes. Clear correlations were observed between the measured and predicted multipole coefficients, demonstrating the strong influence of coil size variations on low order, un-allowed multipole coefficients. In particular, systematic errors were found in the skew sextupole coefficient, which were attributed to tooling asymmetries. This extreme sensitivity of the multipole coefficients on the coil sizes and the tightness of the systematic and rms tolerances suggest that careful controls of the assembly processes be put in place during the production of the nearly 10 000 superconducting magnets needed for the SSC.

REFERENCES

1. P. Schmüser, "Superconducting Magnets for Particle Accelerators," AIP Conference Proceedings, **249**(2), 1099-1158 (1992).
2. A. Devred, T. Bush, *et al.*, "About the Mechanics of SSC Dipole Magnet Prototypes," AIP Conference Proceedings, **249**(2), 1310-1374 (1992).
3. A. Devred, T. Bush, *et al.*, "Review of SSC Dipole Magnet Mechanics and Quench Performance," *Supercollider 4*, 113-135 (1992).
4. J. Strait, D. Orris, *et al.*, "Quench Performance of Fermilab/General Dynamics Built Full Length SSC Collider Dipole Magnets," *Supercollider 4*, 365-372 (1992).
5. M. Anerella, J. Cottingham, *et al.*, "Construction and Test Results from 15 m Long, 50 mm Aperture SSC Collider Dipole Models," *Supercollider 4*, 535-549 (1992).
6. T. Ogitsu, A. Akhmetov, *et al.*, "Mechanical Performance of 5 cm Aperture, 15 m Long SSC Dipole Magnet Prototypes," *IEEE Trans. Magn.*, **3**(1), 686-691 (1993).
7. W. Nah, A. Akhmetov, *et al.*, "Quench Characteristics of 5 cm Aperture, 15 m Long SSC Dipole Magnet Prototypes," *IEEE Trans. Magn.*, **3**(1), 658-661 (1993).
8. P. Wanderer, M. Anerella, *et al.*, "A Summary of SSC Dipole Magnet Field Quality Measurements," *Supercollider 4*, 137-149 (1992).
9. S. Delchamps, M. Bleadon, *et al.*, "Magnetic Field Measurements of Fermilab/General Dynamics Built Full Scale SSC Collider Dipole Magnets," *Supercollider 4*, 251-258 (1992).
10. P. Wanderer, M. Anerella, *et al.*, "Magnetic Design and Field Quality Measurements of Full-Length 50 mm Aperture SSC Model Dipoles Built at BNL," Int. J. Mod. Phys. A (proc. Suppl.) 2B, 641-643 (1993).
11. J. Strait, R. Bossert, *et al.*, "Magnetic Field Measurements of Full Length 50 mm Aperture SSC Dipole Magnets at Fermilab," Int. J. Mod. Phys. A (proc. Suppl.) 2B, 656-658 (1993).
12. Y. Zhao, A. Akhmetov, *et al.*, "Current Dependence of Harmonic Field Coefficients of 5 cm Aperture, 15 m Long SSC Dipole Magnet Prototypes," *IEEE Trans. Magn.*, **3**(1), 674-677 (1993).
13. D. Christopherson, D. Capone, *et al.*, "SSC 40mm Cable Results and 50mm SSC Design Discussions," *IEEE Trans. Magn.*, **27**(2), 1881-1883 (1991).

14. R. Gupta, S. A. Kahn, and G. H. Morgan, "SSC 50 mm Dipole Cross Section," *Supercollider 3*, 587-599 (1991).

15. T. Garavaglia, K. Kauffman and R. Stiening, "Application of the SSCTRK Numerical Simulation Program to the evaluation of the SSC Magnet Aperture," *Supercollider 2*, 59-76 (1990).

16. J. R. Sanford and D. M. Matthews, eds., "Site Specific Conceptual Design Report of the Superconducting Super Collider," SSCL-SR-1056, July (1990).

17. G. Ganetis, J. Herrera, *et al.*, "Field Measuring Probe for SSC Magnets," Proc. 1987 IEEE Part. Acc. Conf., 1393-1395 (1990).

18. A. Devred, J. DiMarco, *et al.* , "Time Decay Measurements of the Sextupole Component of the Magnetic Field in a 4 cm Aperture, 17 m Long SSC Dipole Magnet Prototype," Conference Record of the 1991 IEEE Particle Accelerator Conference, IEEE Catalogue Number 91CH3038-7, 2480-2482 (1991).

19. R. Gupta and A. Jain, "Variation in a_1 Saturation in SSC Collider Dipoles," to appear in the Proceedings of the 1993 IEEE Particle Accelerator Conference, Washington, DC, USA (17-20 May 1993).

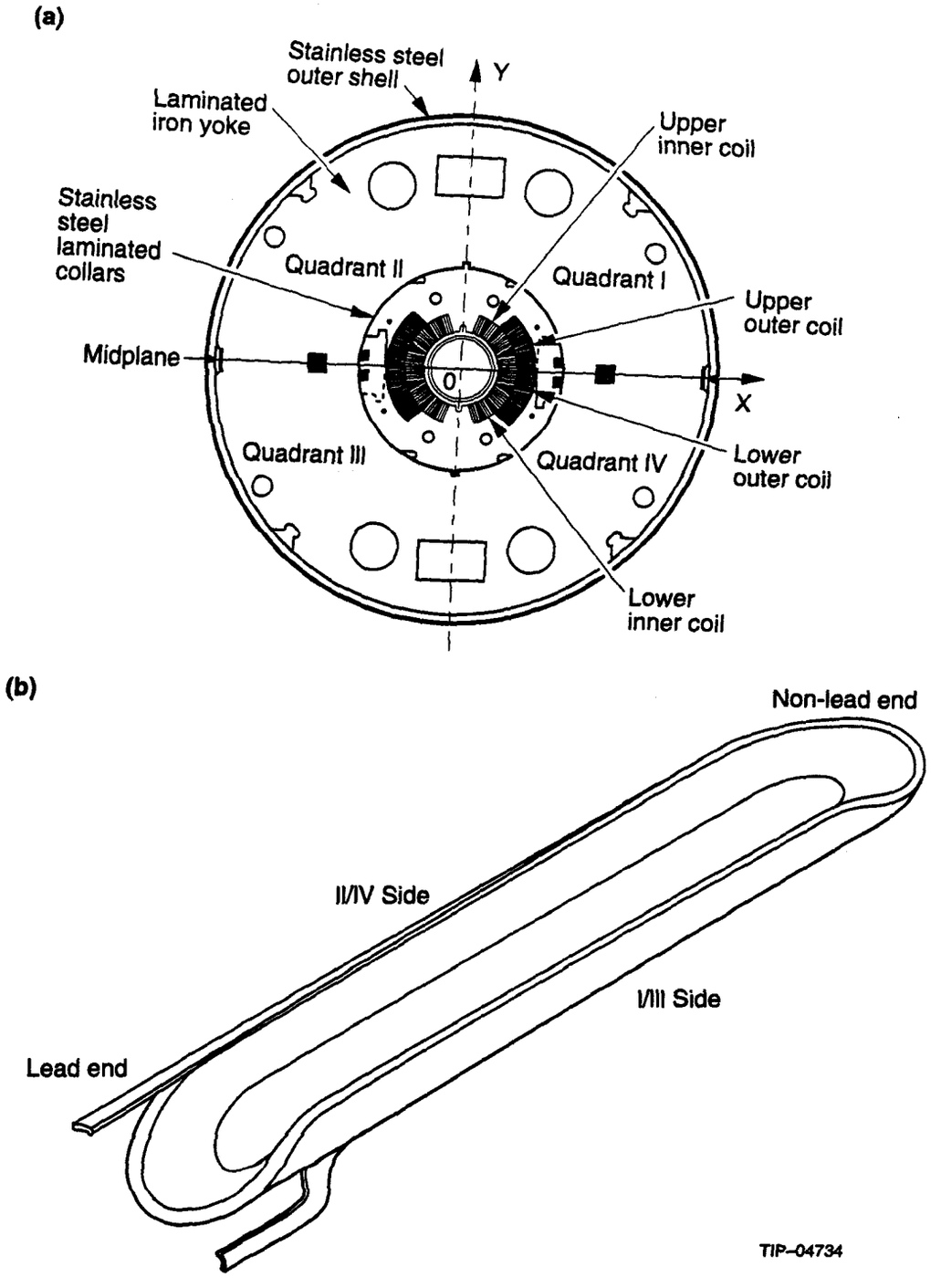

Figure 1. Coil assembly and naming conventions for SSC dipole magnet prototypes: (a) cross-sectional view from the non-lead end of the collared-coil assembly (the non-lead end is the magnet end opposite to that where the current leads are located), (b) perspective view from the lead end of one of the four coils.

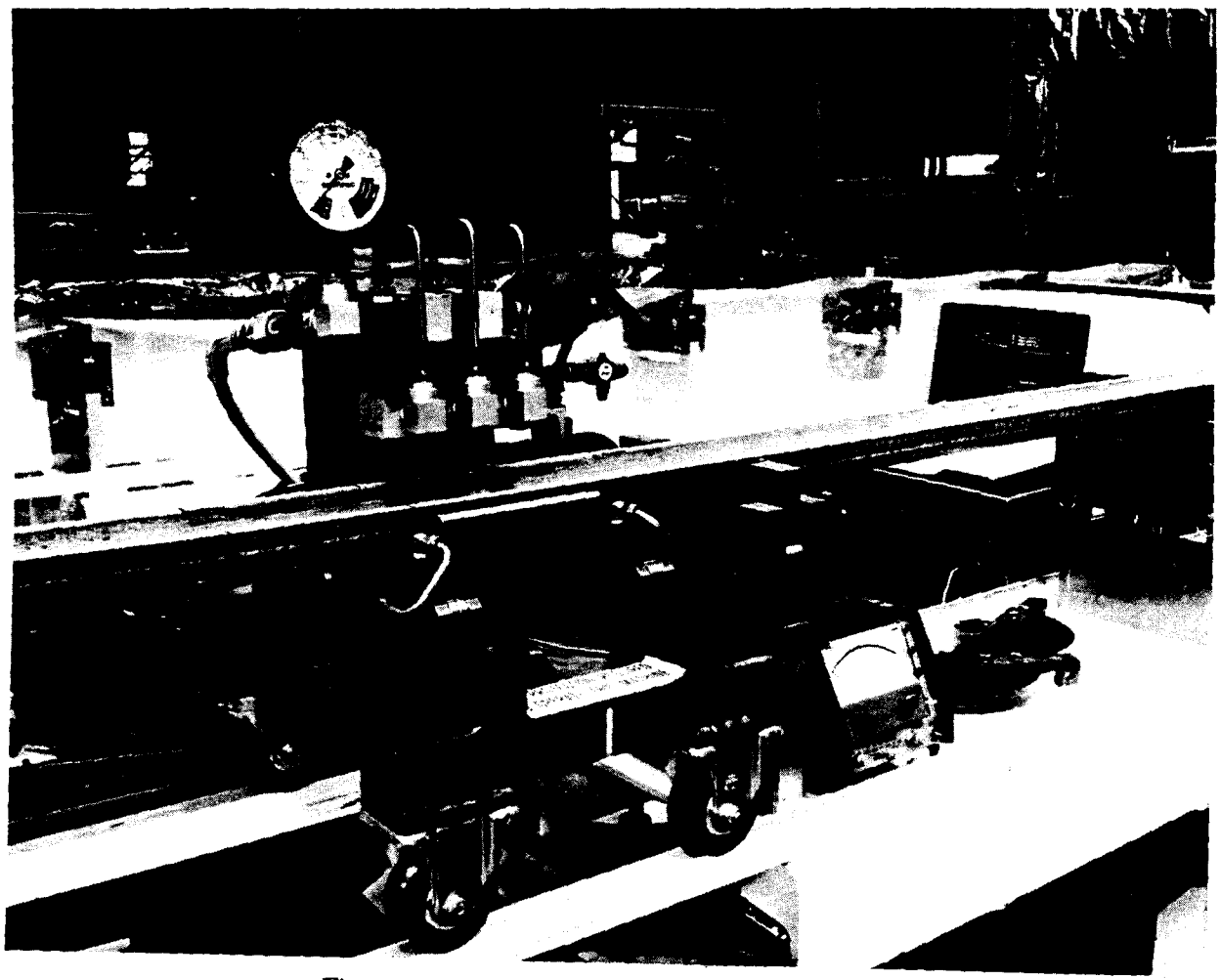

Figure 2. BNL azimuthal coil size measuring device.

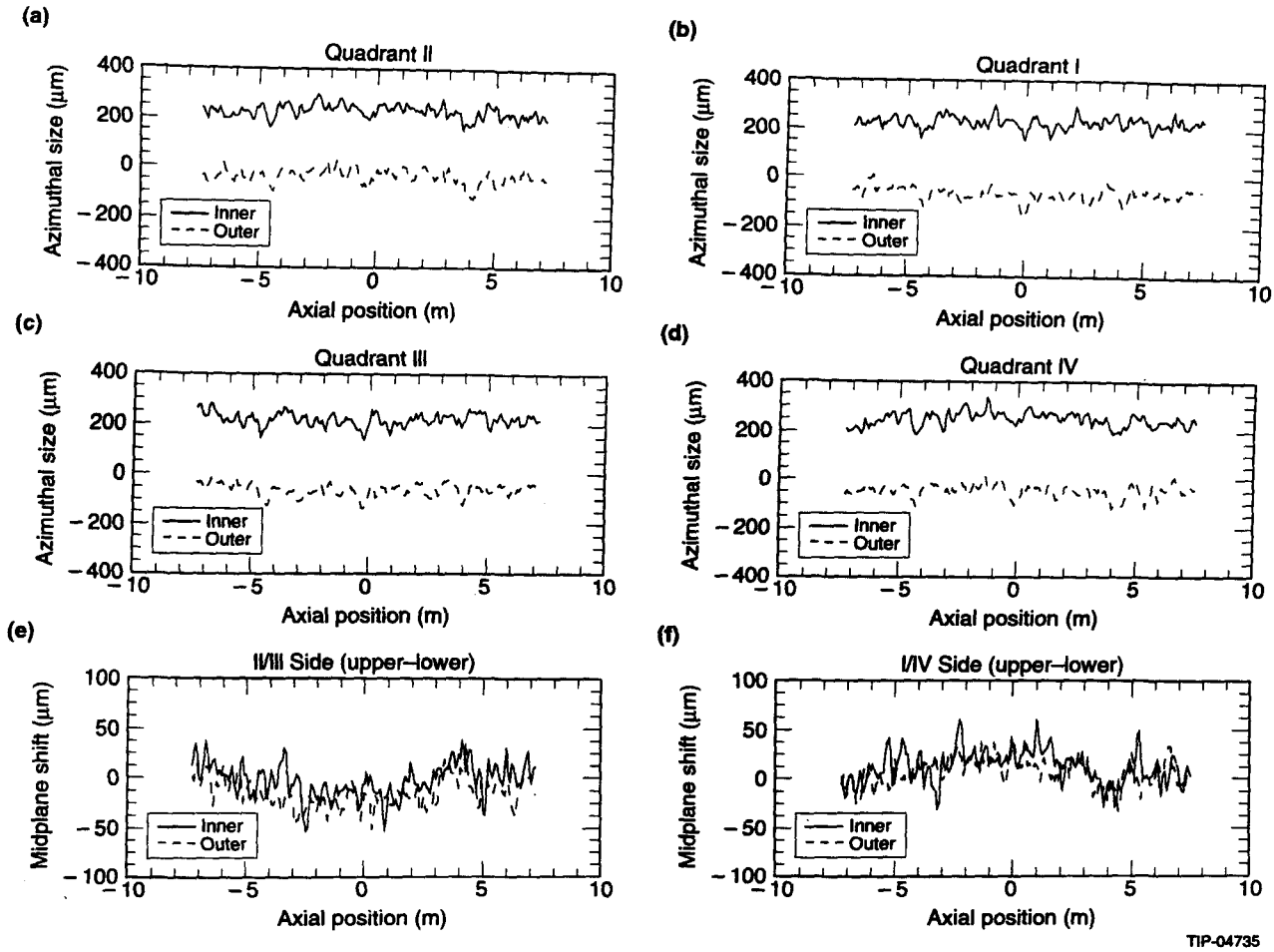

Figure 3. Azimuthal coil size deviations from the master as measured along the length of the four coils assembled in SSC/FNAL dipole magnet prototype DCA315 and the estimated resulting midplane shifts: (a) I/IV side of upper inner and upper outer coils, (b) II/III side of upper inner and upper outer coils, (c) II/III side of lower inner and lower outer coils, (d) I/IV side of lower inner and lower outer coils, (e) estimated midplane shifts in the II/III quadrants, (f) estimated midplane shifts in the I/IV quadrants (for a given side of a given layer, the midplane shift is calculated as upper minus lower azimuthal coil size).

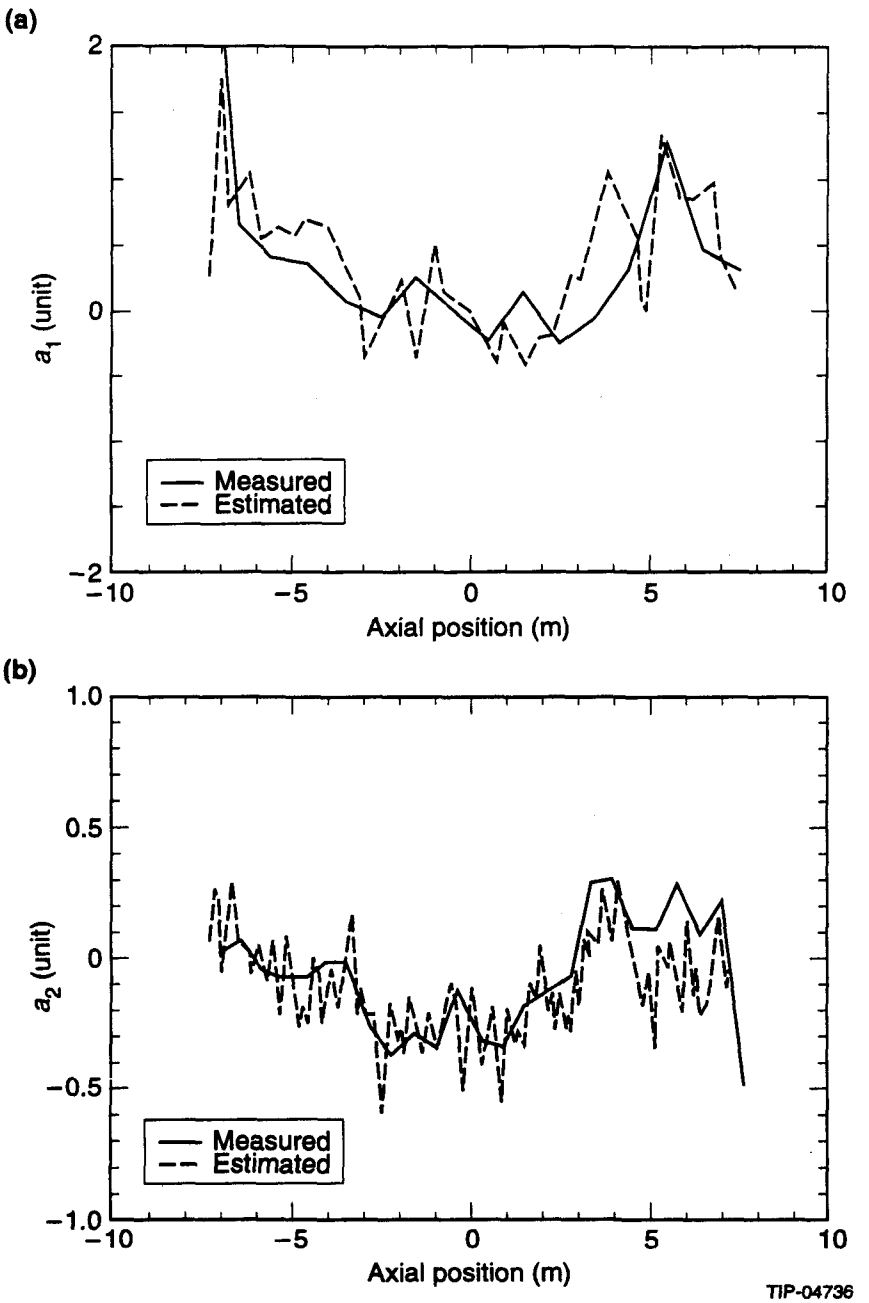

Figure 4. Comparison between measured multipole coefficients and estimated multipole coefficients from the azimuthal coil sizes as a function of axial position: (a) skew quadrupole coefficient along the length of SSC/BNL magnet DCA209, (b) skew sextupole coefficient along the length of FNAL magnet DCA315.

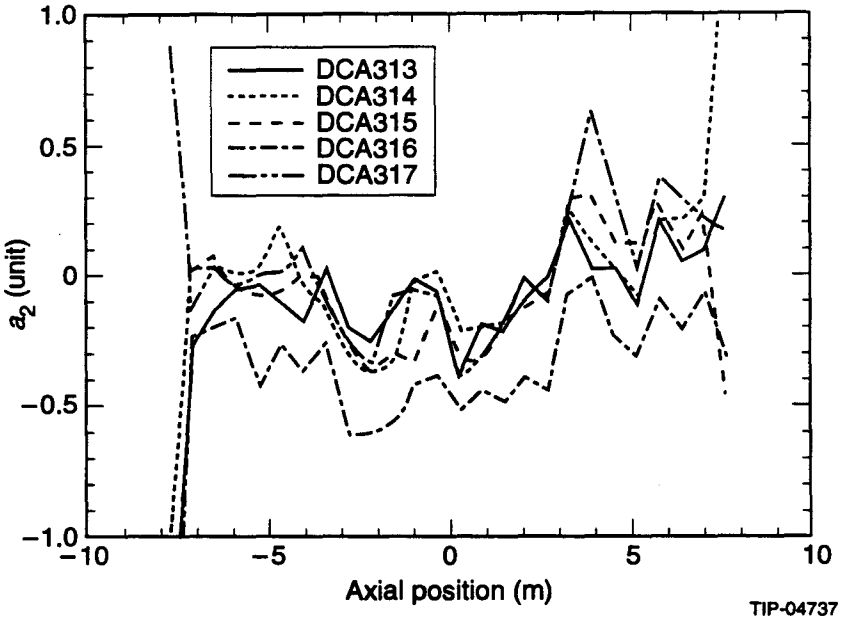

Figure 5. Summary plot of skew sextupole coefficient as a function of axial position for a series of 5 SSC/FNAL dipole magnet prototypes.

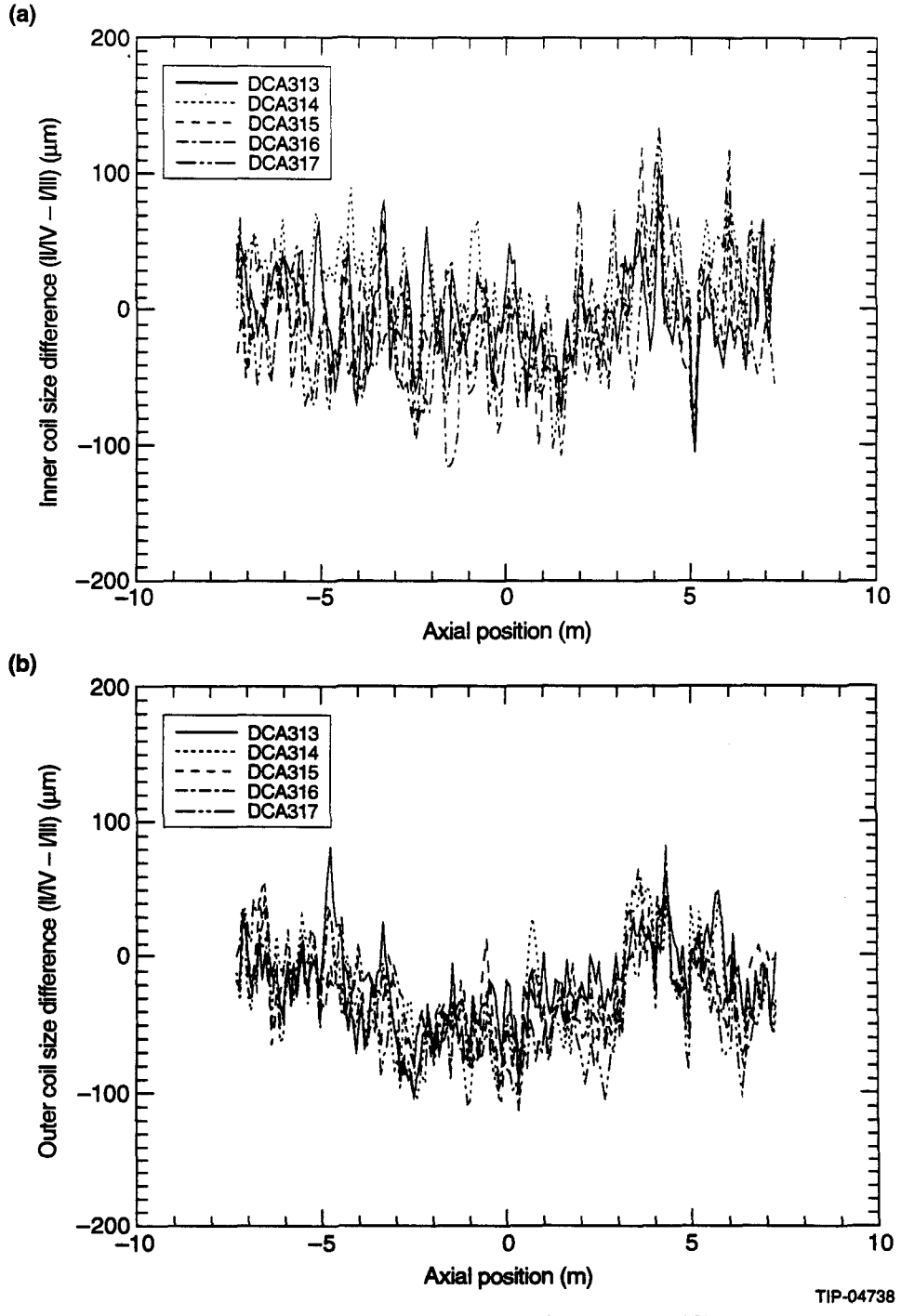

Figure 6. Summary plots as a function of axial position of azimuthal coil size differences between the I/IV side and the II/III side of a representative sample of coils assembled in a series of 5 SSC/FNAL dipole magnet prototypes: (a) inner coils, (b) outer coils.

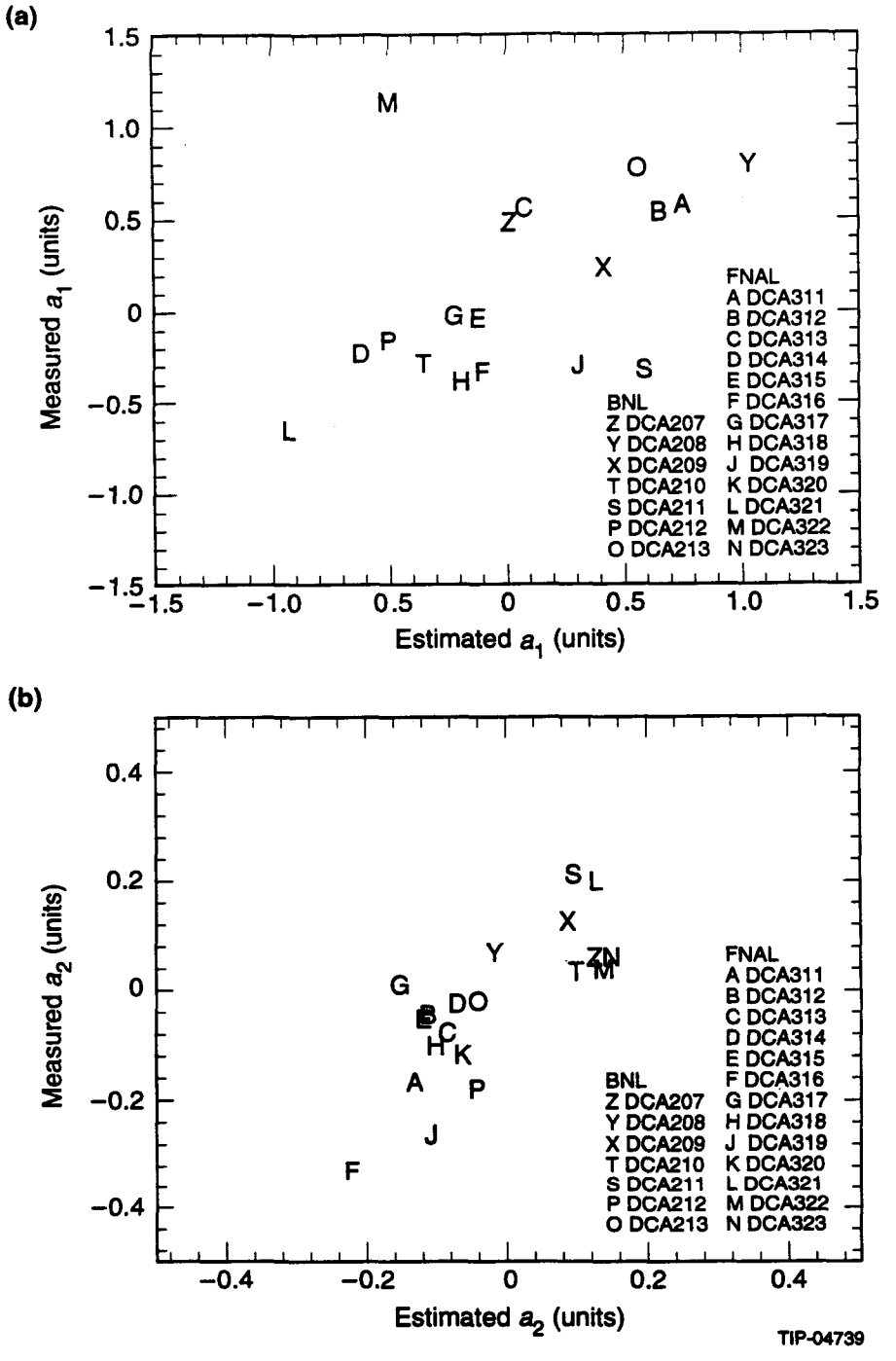

Figure 7. Summary plot of measured multipole coefficients versus estimated multipole coefficients from the coil sizes, averaged over the lengths of a series of SSC dipole magnet prototypes: (a) skew quadrupole coefficient, (b) skew sextupole coefficient. The DCA200 series magnets were built and cold-tested at BNL while the DCA300 series magnets were built and cold tested at FNAL.